Environmental Science Nano

Dynamic Aqueous Transformations of Lithium Cobalt Oxide Nanoparticle Induce Distinct Oxidative Stress Responses of B. subtilis

Journal:	*Environmental Science: Nano*
Manuscript ID	EN-ART-11-2020-001151.R2
Article Type:	Paper

Environmental Significance

Routine environmental nanotoxicology observations are often made without considering the dynamic transformation of the nanomaterials over time, which may lead to observations that cannot be deconstructed adequately into each variable separately. This work investigates the dynamic transform of lithium cobalt oxide ($LiCoO_2$) nanosheets in solutions by both abiotic reactive oxygen species (ROS) generation and Co ion release, and delineates their respective biological impacts in a model bacterium, *B. subtilis*. The observed additional changes in oxidative stress genes and DNA damages in *B. subtilis* coincide with the burst of H_2O_2 in fresh nanoparticle suspensions, which provides direct evidence to connect the abiotic ROS generated by the nanoparticles to the oxidative stress responses in organism. Therefore, the study illustrates a new approach to evaluate nanotoxicity and reveals the importance of evaluating abiotic ROS generation in complex metal oxide nanoparticles.

ARTICLE

Dynamic Aqueous Transformations of Lithium Cobalt Oxide Nanoparticle Induce Distinct Oxidative Stress Responses of *B. subtilis*

Received 00th January 20xx,
Accepted 00th January 20xx

DOI: 10.1039/x0xx00000x

Metti K. Gari[a], Paul Lemke[a], Kelly H. Lu[a], Elizabeth D. Laudadio[b], Austin H. Henke[b], Curtis M. Green[b], Thomas Pho[a,†], Khoi Nguyen L. Hoang[c], Catherine J. Murphy[c], Robert J. Hamers[b], Z. Vivian Feng[a]*

Abstract: Lithium cobalt oxide ($LiCoO_2$), an example of nanoscale transition metal oxide and a widely commercialized cathode material in lithium ion batteries, has been shown to induce oxidative stress and generate intracellular reactive oxygen species (ROS) in model organisms. In this study, we aimed to understand the time-dependent roles of abiotic ROS generation and Co ions released in aqueous medium by $LiCoO_2$ NPs, and examined the induced biological responses in model bacterium, B. subtilis upon exposure. We found that the redox-active $LiCoO_2$ NPs produced abiotic ROS primarily through H_2O_2 generation when freshly suspended. Subsequently, the freshly-suspended $LiCoO_2$ NPs induced additional DNA breakage, and changes in expression of oxidative stress genes in B. subtilis that could not be accounted for by the released Co ions alone. Notably, in 48-hour old $LiCoO_2$ suspensions, H_2O_2 generation subsided while higher concentrations of Co ions were released. The biological responses in DNA damage and gene expression to the aged $LiCoO_2$ NPs recapitulated those induced by the released Co ions. Our results demonstrated oxidative stress mechanisms for bacteria exposed to $LiCoO_2$ NPs were mediated by the generation of distinct biotic and abiotic ROS species, which depended on the aqueous transformation state of the NPs. This study revealed the interdependent and dynamic nature of NP transformation and their biological consequences where the state of NPs resulted in distinct NP-specific mechanisms of oxidative injury. Our work highlights the need to capture the dynamic transformation of NPs that may activate the multiple routes of oxidative stress responses in cells.

Introduction

With the widespread use of nanoscale materials in a variety of fields, research into their biological and environmental impact becomes increasingly important. Several metal oxides, such as TiO_2 and ZnO, due to their applications as photocatalysts[1,2] and in food industry and medical applications[3,4], have been more broadly studied for their biological and environmental impacts. As energy demand grows and fossil fuel resources dwindle, lithium-ion batteries with promising high cell potential, high gravimetric and volumetric capacity, and good cycling performance have taken the center stage recently.[5,6] Consequently, a class of lithium intercalating complex metal oxide nanomaterials has emerged, and is produced in large quantities as battery cathodes.[7] To date, lithium cobalt oxides, $LiCoO_2$, is one of the most ubiquitously used complex metal oxides – from electric vehicles to consumer microelectronic devices. A lack of economic incentives and infrastructure for recycling of these materials[8,9] especially calls for studies to examine the environmental and biological impact of these novel nanomaterials at the end of their life cycle and entrance into the environment.

Metal oxide nanoparticles can lead to cytotoxicity through dissolution of metal ions when placed in media, largely due to their high surface-to-volume ratios. For instance, lithium nickel manganese cobalt oxide has been shown to release toxic levels of nickel, manganese, and cobalt ions that impact bacterial respiration[10,11] and the lifecycle of *Daphnia magna*.[12] Yet, often, the dissolved ions cannot fully recapitulate the biological impacts induced by the nanoparticles. In eukaryotic cells where nanoparticles may be internalized, cytotoxicity has been linked to nanoparticle-induced intracellular reactive oxygen species (ROS) generation and cellular oxidative stress.[13] Metal oxide nanoparticles can induce ROS due to their reactive surfaces, semiconductor electronic properties, or through the release of redox active transition metal ions triggering biomolecule redox reactions.[14] Species, such as superoxide, hydroxyl radical, and hydrogen peroxide, once formed intracellularly at levels that overwhelm the antioxidant systems, often result in oxidative stress exhibited by DNA damage or lipid peroxidation.[14–16] The overproduction of ROS and imbalance of antioxidant defence system can lead to different diseases and cell death.[17] Therefore, examining the mechanisms leading to the production of intracellular ROS and

[a] *Chemistry Department, Augsburg University, Minneapolis, MN 55454*
[b] *Department of Chemistry, University of Wisconsin, Madison, WI, 53706*
[c] *Department of Chemistry, University of Illinois at Urbana-Champaign, Urbana, IL, 61801.*
† Present address: Department of Chemical Engineering, Georgia Institute of Technology, Atlanta, GA, 30332
Electronic Supplementary Information (ESI) available: [details of any supplementary information available should be included here]. See DOI: 10.1039/x0xx00000x

the biological consequences has been proposed as a paradigm for NP toxicity.[1,18]

Some metal oxides, especially semiconductors and photocatalysts, have been shown to spontaneously generate abiotic ROS.[3,18–20] We have previously detected evidence for abiotic ROS produced from lithium nickel cobalt oxide suspensions as the material undergoes incongruent dissolution.[21] The production of ROS, especially superoxide, by TiO_2 has been demonstrated both in response to UV radiation[19,22] and in the dark.[3] These findings raise the question of whether abiotic ROS can directly induce intracellular ROS and trigger oxidative stress responses in model organisms. However, to delineate the biological responses due to ROS vs. metal ions is a challenging question where few studies have attempted to answer,[1] and requires a highly systematic approach.

The question is further complicated by the dynamic nature of both NP transformation and their biological consequences. Although studies have demonstrated the kinetics of metal ion dissolution from metal oxides,[10,11,21,23] few have paid equal attention to monitor the time-dependent ROS generation from nanoparticles.[1] In addition, when organisms are exposed to nanomaterials for extended period of time (*e.g.* days), the studies often result in examining the impact from two coupled variables over time: material transformation and biological responses. Cui et al. demonstrated the dynamic oxidative stress responses from trout gill cells over 48 hrs in a series of elegant single-cell gene expression experiments where different genes were triggered at different time points upon exposure to $LiCoO_2$.[24] These findings further highlighted the needs for investigating the dynamic process of $LiCoO_2$ transformation and the cellular responses.

In this study, we monitor the dynamic transformation of $LiCoO_2$ in terms of Co release and abiotic ROS generation, and examine the biological impact of the transformed $LiCoO_2$ towards a model bacterium, *B. subtilis*. *B. subtilis* is a ubiquitous Gram-positive bacterium that plays major roles in the terrestrial carbon cycle to supply nutrients to plants, and has well-characterized genomes. In contrast to eukaryote cells where nanoparticles can be internalized,[25,26] bacteria do not usually take up the nanoparticles.[10,21,27,28] Therefore, using bacterial models eliminates the complication that material intracellular transformation may differ from that characterized *in situ*. By using species-specific probes and biochemical assays, we aim to detect and identify the spontaneously generated ROS in growth medium as well as intracellular ROS, and establish connections between them. In order to isolate the two time-dependent variables of material transformation and biological responses, we designed experiments to allow $LiCoO_2$ NP suspensions to age in the absence of bacterium for 1 hour and 48 hours, and characterized ion release and abiotic ROS generation at two different time points. We then treated *B. subtilis* with the 1-hr and 48-hr aged $LiCoO_2$ suspensions for a short duration of 30 minutes to minimize the variations in biological responses over time. We assessed oxidative stress markers, such as DNA damage and changes in gene expression in *B. subtilis* upon exposure to $LiCoO_2$ suspensions. Results indicate that additional oxidative stress in bacterium that cannot be fully accounted for by the Co ion released were observed in freshly suspended $LiCoO_2$ solutions, overlapping with the burst of H_2O_2 generation in solution, which suggests that abiotic ROS generation from $LiCoO_2$ indeed led to additional cellular oxidative injury. This study highlights the importance to characterize the dynamic variables independently in order to understanding the multiple paths that lead to oxidative stress responses in organisms.

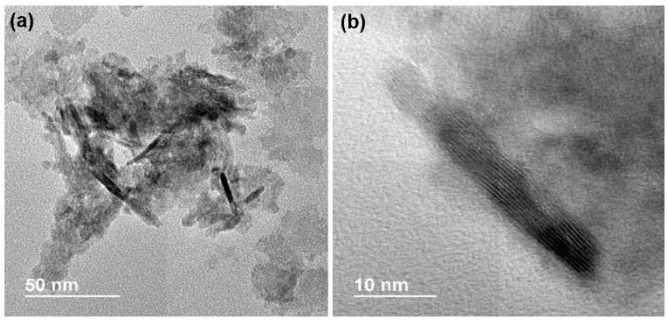

Figure 1. Transmission electron micrographs of pristine $LiCoO_2$ nanoparticles.

Results and Discussion

Characterization of as-synthesized lithium cobalt oxide nanoparticles.

As-synthesized $LiCoO_2$ nanoparticles were characterize morphologically and structurally. Micrograph images from TEM show the typical morphology of these nano-structures (Fig 1) where a high magnification view of one of such structures shows the sheet-like morphology (Fig 1b). BET analysis yielded a surface value of 125 m^2/g for the $LiCoO_2$ nanoparticles. The collected powder XRD pattern, published previously,[29] can be indexed to the $R\bar{3}m$ space group, as expected for this crystal structure. However, we note that the as-synthesized $LiCoO_2$ without the high temperature annealing step has lower crystallinity, which more-closely represents spent cathode materials after numerous electrochemical cycles, the condition at which environmental exposure occurs. Dynamic Light Scattering (DLS) measurements of 5 mg/L suspensions of particles in ultrapure water yielded diffusion coefficient and ζ-potential values of 0.8 ± 0.1 $\mu m^2/s$ and -2.0 ± 1.0 mV, respectively. We report diffusion coefficient (in $\mu m^2/s$) of these particles as an indicator for size because it is a direct measurement from the DLS, while hydrodynamic diameter is calculated from diffusion coefficient assuming the particles to be spherical in shape, a poor assumption to make in this case.

$LiCoO_2$ dissolution and the release of cobalt ion over time.

Previously, both experimental[25,30] and computational studies[31] have demonstrated that $LiCoO_2$ nanoparticles can undergo partial dissolution in aqueous media. The extent and the kinetics of dissolution are dependent on nanomaterial surface properties, solution pHs and constituents. Prior studies[10–12,25,26] examining the biological impact of this class of complex metal oxides with various model organisms have repeatedly indicated that the amount of Li^+ released, although significantly higher than those of the transition metal ions (*e.g.* Co^{2+}, Ni^{2+} and Mn^{2+}), has minimal impact to the

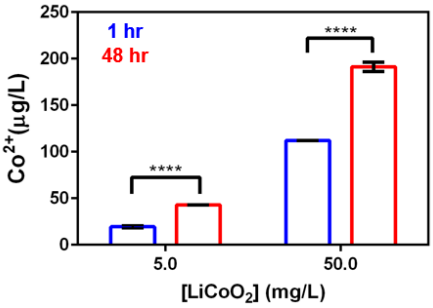

Figure 2. Co ion dissolution from $LiCoO_2$ upon suspension in bacterial growth minimal medium with 10 mM dextrose for 1 hr (blue) vs. 48 hrs (red) quantified by ICP-MS (n = 3, **** for $P < 0.0001$ with two-way ANOVA with Sidak's multiple comparison test). Error bars represent standard error of means.

organisms tested, *B. subtilis* included.[11] Therefore, we focus on the specific impact of cobalt ion released from the material in this study. ICP-MS analysis was used to quantify the time-dependent cobalt ion dissolution in the $LiCoO_2$ suspensions in a *B. subtilis* growth minimal medium. Fig 2 shows the amount of Co^{2+} released from 5.0 and 50.0 mg/L $LiCoO_2$ after suspension for 1-hr (blue) and 48-hr (red) periods. As expected, higher amounts of Co^{2+} ions were released in solution at the higher $LiCoO_2$ concentration, and as the nanoparticles were suspended for a longer period of time compared to a freshly suspended (1-hr) $LiCoO_2$ suspension.

$LiCoO_2$ generates abiotic ROS in growth medium.

In addition to ion release, previous investigations of complex metal oxides have revealed that, depending on the composition of the material, reactive oxygen species can be generated spontaneously upon material dissolution.[21] ROS are known to cause oxidative stress resulting in cellular damage in bacteria.[32] Therefore we aimed to first detect and identify if any ROS were generated simultaneously by $LiCoO_2$ nanoparticle suspensions in bacterial growth media.

Fig 3 shows the results from a selection of ROS probes used to detect and identify the presence of specific species in $LiCoO_2$ suspensions over time. Amplex Red™ assay,[33,34] a horseradish peroxidase (HRP)-based assay that has been previously applied to detect H_2O_2 generated from TiO_2 nanoparticle suspensions[35] was used to detect and quantify H_2O_2 in $LiCoO_2$ NP suspensions. Fig 3a shows results from the quantification of H_2O_2 using Amplex Red, indicating the formation of abiotic ROS in bacterial growth medium with $LiCoO_2$ suspension, and the identity of the ROS is likely to be H_2O_2. Statistical analysis shows that the amounts of H_2O_2 generated from the freshly (1-hr) suspended $LiCoO_2$ NPs at both 5 and 50 mg/L level are significantly different from that of the control (blank medium), and the amounts of H_2O_2 detected in a 48-hr old suspension are significantly lower than those from freshly suspended $LiCoO_2$ at both concentrations ($P < 0.0001$, two-way ANOVA). The results suggest that ROS is indeed generated at an early stages of $LiCoO_2$ NP dissolution in aqueous media, yet the abiotic ROS signal decreases over time as the $LiCoO_2$ is left in solution for longer period of time.

Although the use of fluorescent probes is a common and effective approach to detecting ROS,[36] one of many possible errors that can

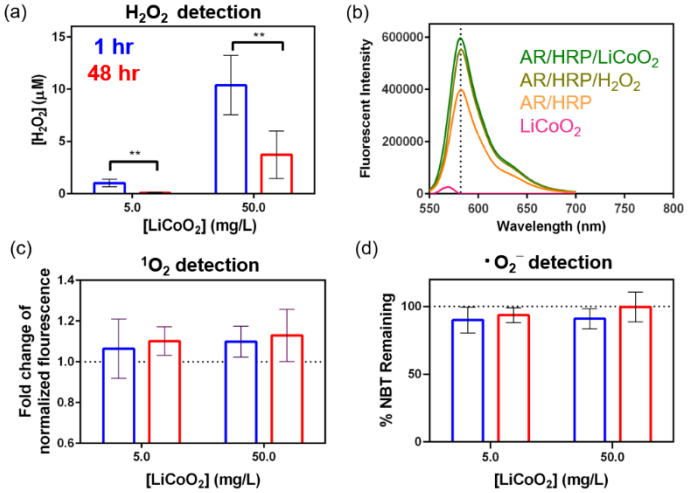

Figure 3. Abiotic ROS detection in $LiCoO_2$ suspension after 1-hr (blue) and 48-hr (red) in minimal media with 10 mM dextrose. (a) Quantification of hydrogen peroxide generated from $LiCoO_2$ suspensions monitored by Amplex Red dye (n = 4, ** for $P < 0.01$ with two-way ANOVA with Sidak's multiple comparison test), (b) Representative fluorescence spectra of 100 µM Amplex red (AR) and 0.1 unit·mL-1 horseradish peroxidase (HRP) solution after 1 hr exposure through a filter membrane to $LiCoO_2$ nanoparticles and/or 1 µM H_2O_2 standard solution. (c) Normalized fluorescence signal from singlet oxygen sensor green (SOSG) for singlet oxygen detection. (d) Attenuation in absorbance at 259 nm of nitroblue tetrazolium solutions (NBT) upon exposure to $LiCoO_2$ solutions for superoxide generation detection.

arise when using such a probe molecule is false-positive detection via the probe reacting at a potentially catalytic surface, such as $LiCoO_2$ NPs.[37] To ensure that positive results of the Amplex Red assay were due to the transformation of Amplex Red to resorufin upon reaction with free H_2O_2 and not on the nanoparticle surfaces, we performed diffusion assays with $LiCoO_2$ suspension. We assembled an apparatus (Fig S1) to spatially separate the $LiCoO_2$ nanoparticles from the Amplex Red-HRP solution using a finely porous hydrophobic filter membrane. Fluorescence of the resulting solution above the filter membrane (*i.e.* no direct particle exposure) is used to detect H_2O_2 with 1 µM H_2O_2 below the filter membrane as a standard. Under this experimental design, an increase in fluorescence would be from the reaction of Amplex Red with free H_2O_2 and not with the nanoparticle surfaces, assuming i) H_2O_2 readily diffuses through the membrane, ii) $LiCoO_2$ cannot diffuse through the membrane (25 nm pores are small relative to particle diameter), and iii) HRP will not appreciably diffuse through the membrane within the time scale of the experiment. Although Amplex Red may diffuse through the membrane, conversion to the fluorescent product requires the HRP catalyst. Although we expect cobalt ions may also diffuse through the membrane, Co^{2+} alone did not induce fluorescence intensity change with Amplex Red in control experiment. Fig 3b shows representative fluorescence spectra of each sample tested with the normalized fluorescence intensity normalized to the background in the inset. The presence of $LiCoO_2$ NPs results in an increase in fluorescence compared to the AR-HRP control solution. Addition of 1 µM H_2O_2 spike produces a similar effect, indicating that H_2O_2 diffuses through the membrane over the 1 hr period and reacts with AR-HRP. The presence of $LiCoO_2$ particles alone (no AR-HRP) shows no fluorescence, with small background intensity coming from scattering of the excitation. These results show that positive

detection of H_2O_2 in our Amplex Red experiment is indeed due to the presence of abiotic H_2O_2 and not direct interaction of Amplex Red with the $LiCoO_2$ NPs.

The singlet oxygen sensor green (SOSG) fluorescence dye was employed to discern the production of singlet oxygen in the $LiCoO_2$ dissolution and is highly specific to singlet oxygen detection. This dye manifests in weak blue color initially and emits green fluorescence with the presences of singlet oxygen (excitation/emission: 504/525 nm).[19] Fig 3c shows that the normalized fluorescence signals indicating the $LiCoO_2$ suspension at different time points did not produce significant amount of singlet oxygen in solution when compared to control.

Lastly, the generation of superoxide was monitored by observing the reduction in absorbance at 259 nm of a nitro blue tetrazolium solution (NBT). Superoxide, if present, can react with NBT to form a precipitate, formazan, resulting in a decrease in the absorbance at 259 nm.[35] Fig 3d shows that the NBT absorbance signal does not decrease in the presence of $LiCoO_2$ suspension regardless of concentration and time-point, which suggests no superoxide formation by the $LiCoO_2$ nanoparticles in solution.

Results shown in Fig 3 overall confirms that ROS is generated by $LiCoO_2$ suspension in bacterial growth medium. More significantly, we were able to identify the species generated as hydrogen peroxide and quantify its concentrations in $LiCoO_2$ suspensions. The H_2O_2 diffusion experiment also critically illustrated that the observed fluorescence signal using a dye was not the results of optical interference by the nanomaterials, or by nanoparticle surface catalyzed chemical reaction of the dye molecules. The chemical nature of $LiCoO_2$ determines that cobalt is in the Co^{3+} state. In fact, we have detected a Co(III)-EDTA complex spectroscopically when $LiCoO_2$ NP was dissolved in the presence of EDTA in solution (Fig S2). Upon dissolution, Co^{3+} is likely to reduce to the more soluble form of Co^{2+}. We have also observed the redox activity of $LiCoO_2$ upon suspension in aqueous media is able to oxidize the electron transporters, nicotinamide adenine dinucleotide (NADH) (unpublished). Therefore, we hypothesize that the Co(III) reduction is then likely to trigger water oxidation and generate H_2O_2.

Table 1. Comparison of $LiCoO_2$ nanoparticle properties at various stages of suspension in aqueous media.

		Media-suspended	
	As-synthesized	1-hr	48-hr
z-potential (mV)	-2.0 ± 1.0	-28 ± 2	-25 ± 4
Diffusion coefficient ($\mu m^2/s$)	0.8 ± 0.1	0.9 ± 0.5	1.0 ± 0.2

Interestingly, by examining the solution constituents of the nanoparticle suspension at two different time points (1-hr vs. 48-hr), we were also able to probe the dynamic process of both ion release and ROS formation from complex metal oxides in aqueous medium. Although studies have indicated the importance to monitor ion release from metal or metal oxide nanoparticles through dissolution over time because of ion-induced toxicity to organisms,[10,11] there have been few studies examining abiotic ROS formation over time. We note that parallel attention is needed to monitor the generation of abiotic ROS in these nanoparticle suspensions over time as well as ion release, in order to develop a holistic view of the chemistry of material transformation.

On the other hand, the $LiCoO_2$ particles after suspension in media do not undergo noticeable changes morphologically compared to those freshly synthesized (Fig S3). The layered structure of the nanosheets remains visible. ζ-potential (ZP) analysis of medium-exposed $LiCoO_2$ also yielded comparable values as shown in Table 1. The exposed particles have more negative ZP values than that of the pristine particles, which is expected due to the surface-adsorbed phosphate species to $LiCoO_2$.[30] The diffusion coefficients of the medium-exposed particles after 1 hr and 48 hr exposure are also comparable with that of the pristine particles, suggesting minimal variations in particle size. This experimental evidence suggests that any transformations due to exposure to the medium is likely surface limited.

$LiCoO_2$ impacting bacterial viability

Previous studies have shown that transition metal oxides do not enter bacterial cells, in contrast to their interactions with eukaryote cells.[10,25] Instead, the ions released from these materials often can recapitulate the impact on bacterial respiration[10,11,38] and viability.[39] Therefore, we studied the effect of $LiCoO_2$ nanoparticles and the corresponding amount of ions released over time by monitoring the viability of *B. subtilis*. A growth-based viability (GBV) analysis was performed to quantify the relative amount of viable bacterial cells under different exposure conditions to $LiCoO_2$ nanoparticles by the periodic measurement of OD_{600}.[40] In this assay, the viability of bacterial cultures exposed to nanoparticles is assessed by comparing the delay in the culture regrown in fresh nutrient-rich media against a preconstructed calibration curve relating the delay to the number of viable cells. The assay is especially effective in evaluating nanotoxicity to bacterial species because it eliminates the concerns for nanomaterial aggregation in nutrient-rich media, and reduces optical interferences by nanomaterials in normal growth assays. We hypothesized that cobalt dissolution contributes significantly to the

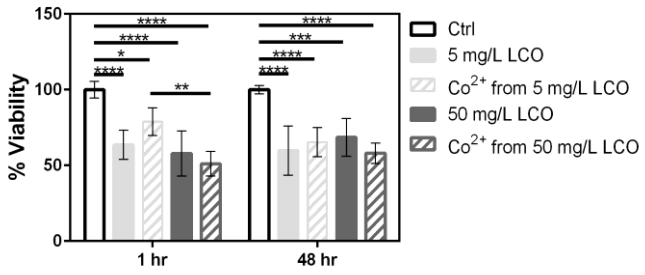

Figure 4. Bacterial viability of B. subtilis upon exposure to 5 and 50 mg/L of $LiCoO_2$ or their corresponding amount of Co^{2+} ion released at 1-hour and 48-hour time points (n = 4, one-way ANOVA with post-hoc Tukey's multiple comparisons test, * for $p < 0.05$, ** for $p < 0.01$, *** for $p < 0.001$ and **** for $p < 0.0001$).

impact of the bacterial population. Hence, viability comparisons were made between the $LiCoO_2$ suspensions and their corresponding amounts of dissolved cobalt ions at different time-points and concentrations. Fig 4 shows that at both time points and both concentrations examined, the bacterial viabilities have fallen to 50~70% compared to unexposed cells. The concentrations and the age of the $LiCoO_2$ suspension did not yield significant difference in the level of toxicity. Moreover, no significant differences in viability were observed induced by the $LiCoO_2$ and the cobalt ion released (solid vs. shaded bars) at each concentration and time point. In fact, when examining the bacterial viability as a function of $LiCoO_2$ (Fig S5a) and of Co^{2+} (Fig S5b) at wider concentration ranges, we observed that the correlation between the concentrations and viability is non-linear, which may explain the similarities in bacterial viability between the 5 and 50 mg/L $LiCoO_2$ treatments at various time points. Overall, the presence of $LiCoO_2$ and the released Co^{2+} both reduced viability of the bacterium. The released Co^{2+} recapitulate the impact of $LiCoO_2$ to *B. subtilis* viability at the concentrations and time points examined.

Bacterial intracellular ROS and oxidative stress responses induced by $LiCoO_2$

Cell viability and toxicity studies, although important indicators of the nanomaterial's impact, are often end-point measurements that do not provide detailed mechanistic insights of the more subtle biological changes. Hence, we examine the biological impact to $LiCoO_2$ by characterizing Co ion internalization and intracellular ROS generation guided by the observations of ion release (Fig 2) and the abiotic ROS generation (Fig 3). We first test the hypothesis that as the amount of Co^{2+} released in solution increases over time, a higher influx of Co^{2+} is internalized in bacterial cells. Therefore, the $LiCoO_2$ dissolution will likely result in increased metal ion influx in bacterial cells. Newport Green™ DCF is a cell permeable fluorescent dye used for the detection of divalent metal ion internalization in cells[41] and has been previously successfully employed in bacterial species to monitor the internalization of divalent transition metal ions.[39,42] Fig 5 shows an increase in fluorescence signal at increasing $LiCoO_2$ concentrations, revealing that, at both 5 and 50 mg/L of $LiCoO_2$, there is a significant amount of Co^{2+} uptake in cells. Furthermore, significantly higher fluorescence signals were observed as the

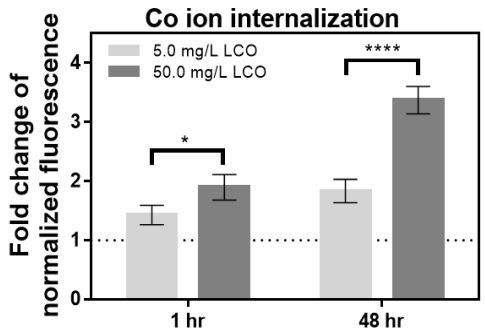

Figure 5. Normalized fluorescence signal from Newport Green™ dye for Co^{2+} ion internalization in *B. subtilis* upon exposure to 1-hour, and 48-hr old $LiCoO_2$ suspension in the minimal growth medium (n = 4, unpaired *t*-test with Welch's correction, * for $p < 0.05$, and **** for $p < 0.0001$).

$LiCoO_2$ CO suspension aged. This observation is consistent with the ICP-MS analysis (Fig. 2) which reported an increased cobalt ion release over time.

The detection of H_2O_2 in solution from $LiCoO_2$ suspension led us to examine the oxidative stress responses in bacterial cells. Intracellular ROS studies were conducted to understand how bacterial cells combat the oxidative stress upon exposure to $LiCoO_2$. $DCFH_2$-DA, a generic ROS probe, was used for the detection of intracellular ROS in *B. subtilis* upon 30-min exposure to $LiCoO_2$ suspensions that were 1 hr- and 48 hr-aged (Fig 6a). Results show a clear increase in fluorescence signals from bacterial cells grown in media with increasing $LiCoO_2$ concentrations, which confirms the generation of intracellular ROS in *B. subtilis* under these exposure conditions. Similarly, intracellular ROS signals have been detected previously when trout gill cells were exposed to $LiCoO_2$ suspensions.[25] Interestingly, in contrast to the abiotic ROS signals from growth media (Fig 3a), intracellular ROS signals do not exhibit a time-dependent manner for $LiCoO_2$ NPs suspended for different durations (data replotted in Fig S6a for comparison) ($P > 0.05$ with two-way ANOVA). Although abiotic H_2O_2 is generated with an initial burst when freshly suspended, then decays at 48-hr, the intracellular ROS signals in bacteria remain rather constant. Therefore, it is critical to note that the biotic and abiotic ROS signals are generated through different mechanisms. Their correlation and interdependent nature will be discussed below.

Furthermore, in contrast to the lack of abiotic superoxide detected in solution (Fig 3d), Fig 6b shows fluorescence measurements from

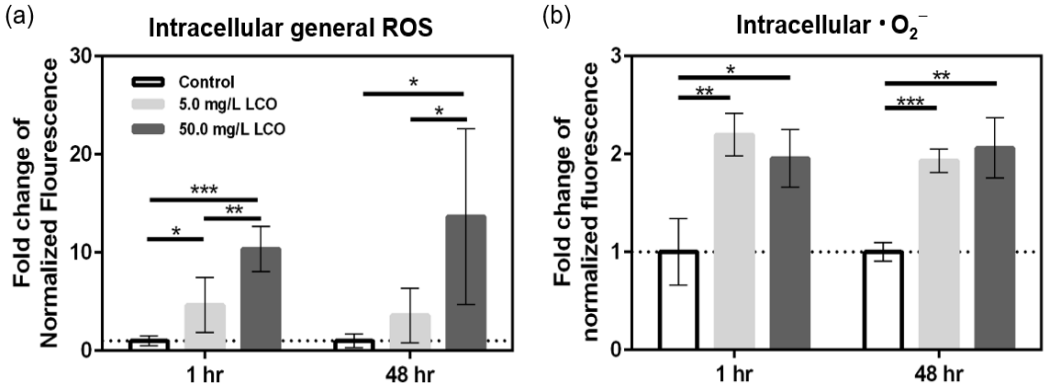

Figure 6. Intracellular ROS detection in *B. subtilis* grown in $LiCoO_2$ suspensions in minimal media with 10 mM dextrose. (a) Normalized fluorescence signal from DCF-DA dye, and (b) normalized Fluorescence signal from Dihydroethidium (DHE) dye for intracellular superoxide in *B. subtilis* (n = 6, one-way ANOVA with Tukey's multiple comparisons test).

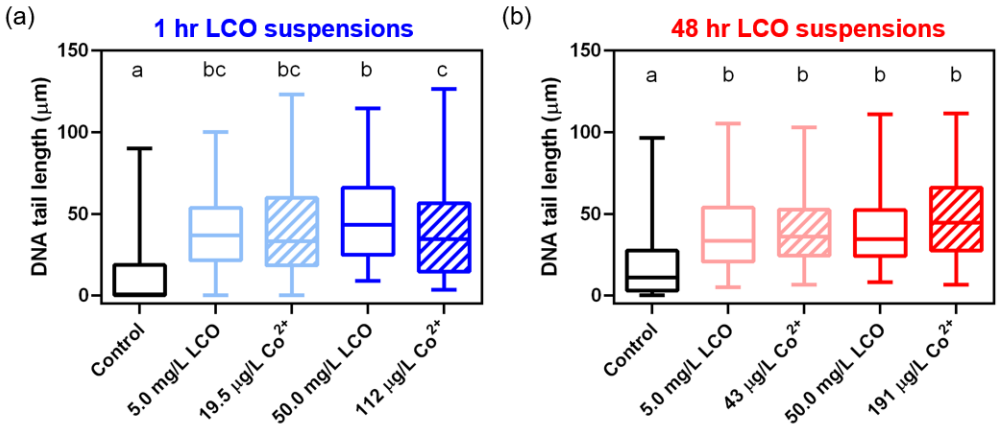

Figure 7. Comparison of bacterial DNA tail lengths resulted from single-cell gel electrophoresis analysis of *B. subtilis* upon exposure to (a) 1-hour, and (b) 48-hour $LiCoO_2$ NP suspensions. Shaded symbols represent treatments with equivalent amount of Co^{2+} released from $LiCoO_2$ NPs (n > 200; D'Agostino & Pearson normality test was first used to test for normal distribution; "a", "b", "c" denote statistically significant differences using the non-parametric Kruskal-Wallis tests with Dunn's multiple comparison).

the Dihydroethidium (DHE), a probe sensitive to detect intracellular superoxide,[43,44] suggesting the generation of superoxide in *B. subtilis* grown in $LiCoO_2$ suspensions. Interestingly, the intracellular superoxide signals are neither concentration-dependent, nor $LiCoO_2$ -suspension age-dependent (replotted in Fig S6b) ($P > 0.05$ with two-way ANOVA). In the intracellular environment, superoxide is often formed on the oxygen reduction pathway in a single-electron transfer redox reaction when molecular O_2 adventitiously oxidizes redox enzymes.[45,46] Intracellular superoxide, once formed, can be further reduced to H_2O_2 in another one-electron redox process by superoxide dismutase, SOD.[45] Therefore, the generation and consumption of superoxide are likely to be a dynamic process in *B. subtilis*, which may explain the concentration- and suspension-age-independent behavior observed.

Because H_2O_2 can both permeate through the cell wall from $LiCoO_2$ -containing media and be generated from intracellular superoxide reduction, we investigate the fate of intracellular H_2O_2 in *B. subtilis* using a luminescence dye, ROS-Glo™. Unfortunately, due to an optical interference of the dye in the presence of $LiCoO_2$ NPs, indicated by a color change upon mixing, we were unable to conduct the parallel experiment using $LiCoO_2$ NP-treated bacterial cells. Instead, we conducted experiments by dosing the bacterial culture with 30 μM H_2O_2 to observe the luminescence signals from cells upon treatment. The results from cells spiked with H_2O_2 distinctively show that H_2O_2 is not accumulated in bacterial cells, but is likely further converted (Fig S6). The intracellular concentration of H_2O_2 has been previously described as the difference between influx+intracellular formation and efflux+scavenging.[47] The diffusion rate of H_2O_2 across bacterial membrane can be matched by the rate of Alkyl hydroperoxide reductase (Ahp) or catalase turnover at the micromolar concentration levels of H_2O_2, which lowers intracellular H_2O_2 concentrations than that of the external environment.[48] Our results from ROS-Glo™ indicate a dynamic and active conversion of H_2O_2 in *B. subtilis*.

$LiCoO_2$ induces bacterial DNA damage and changes in oxidative stress genes.

Intracellular H_2O_2 can either be converted to H_2O and O_2 by catalase, or react with labile Fe^{2+} in the intracellular environment through the Fenton reaction to produce ·OH.[34,48] Therefore, we further investigate the downstream biological impact of intracellular ROS. Although H_2O_2 does not normally damage DNA directly,[45] the highly transient and electrophilic ·OH is known to attack the electron-dense DNA molecules that lead to DNA damage.[49] Hence, although it is experimentally challenging to directly detect ·OH intracellularly, by monitoring the extent of bacterial DNA damage, we can probe the impact of this intracellular ROS. Single-cell gel electrophoresis (i.e, comet assay) at neutral pH environment is a sensitive method to detect and compare the extent of double-strand DNA breakage caused by exposure to $LiCoO_2$ NPs. The fragmented bacterial DNA exhibits a tail-like morphology upon nucleic acid staining, and the tail length is indicative of the extent of damage.[50,51] We have previously used this method to assess the genotoxicity of nanomaterials to bacteria successfully.[11,42]

Fig 7 shows the resulting DNA tail length analysis of *B. subtilis* upon exposure for 30 minutes to $LiCoO_2$ NP suspensions that are 1-hr (blue) or 48-hr (red) old, as well as the corresponding amounts of Co^{2+} released (shaded) at respective concentrations and time points. Because the DNA tail length is indicative of the extent of DNA damage, analysis of DNA tail length shows that both the $LiCoO_2$ NPs and Co^{2+} have induced significant DNA damage ($p < 0.0001$, non-parametric one-way ANOVA test). This observation suggests the presence of ·OH in *B. subtilis* upon exposure to both the $LiCoO_2$ NPs and Co^{2+}.

Transition metals are well-known to induce oxidative stress through generating intracellular ROS.[34] Such properties of metal or metal oxide nanoparticles have also been explored as antibiotic agents towards bacterial species.[52–54] Due to their multivalent nature, many transition metal ions can trigger redox chemistry in cellular environment by disrupting enzymatic functions and damaging biomolecules, such as proteins and DNA. In vitro studies have shown that Co^{2+} have been linked to single-strand breaks in salmon sperm DNA through Fenton-like reactions, and to create putative intrastrand cross-links of DNA.[55] Although Co(II) did not generate

Table 2. Heat map of changes in expression levels of selective genes related to oxidative stress, metal regulation, and DNA repair mechanisms in *B. subtilis* upon exposure to 1-hr and 48-hr $LiCoO_2$ suspensions and their corresponding amounts of Co ion released.

1-hr LCO				48-hr LCO					
5 mg/L		50 mg/L		5 mg/L		50 mg/L			
LCO	Co^{2+}	LCO	Co^{2+}	LCO	Co^{2+}	LCO	Co^{2+}		
-2.3	-0.5	-2.3	-0.5	-3.2	-2.9	-3.2	-2.9	*katA*	Oxidative stress
-0.5	0.2	-1.4	-0.5	-0.9	-0.6	-2.2	-1.8	*ahpC*	
0.3	0.3	-0.5	0.2	0.0	0.2	-0.9	-0.6	*ohrA*	
-0.1	-1.6	0.3	0.3	0.2	0.2	0.0	0.2	*tpx*	
0.2	-0.5	-0.1	-1.6	-0.3	0.1	0.2	0.2	*perR*	
-1.4	-0.5	0.3	0.5	-2.2	-1.8	-0.1	0.0	*mrgA*	
0.3	0.5	0.2	-0.5	-0.1	0.0	-0.3	0.1	*fur*	
0.5	0.0	0.5	0.0	0.3	0.7	0.3	0.7	*sodA*	
0.1	0.3	0.1	0.3	0.5	0.4	0.5	0.4	*czcD*	Metal regulation
-0.2	0.3	-0.2	0.3	0.3	0.2	0.3	0.2	*mutM*	DNA repair
-0.2	0.3	-0.2	0.3	0.3	0.3	0.3	0.3	*recJ*	
0.1	0.5	0.1	0.5	0.2	0.1	0.2	0.1	*ruvA*	
-0.1	0.2	-0.1	0.2	0.1	-0.4	0.1	-0.4	*lexA*	
0.0	0.4	0.0	0.4	0.2	0.1	0.2	0.1	*recU*	
-0.1	0.4	-0.1	0.4	0.2	0.1	0.2	0.1	radA	

-4 -2 0 2 4

significant amount of ·OH when reacting with H_2O_2, a Co(I) mediated Fenton-like reaction has been proposed.[56] In addition, Co^{2+} can preferentially bind to specific sequences in DNA, *e.g.* the 5' G of GG sequences or the middle G of GGG.[34] We have also observed double-strand breakage induced by Ni^{2+} and Co^{2+},[11] as well as a variety of oxidative stress-related putative DNA adducts in two bacterial species upon exposure to nanoscale nickel manganese cobalt oxides in previous studies.[42] Taken together, transition metal oxides generating multivalent metal ions that can enter bacterial cells and lead to bacterial DNA damage through Fenton-like reactions is likely a common toxicity mechanism for such materials.

Interestingly, when comparing the DNA tail lengths induced by $LiCoO_2$ NPs vs. the Co^{2+} alone, we observe different trends depending on the age of the $LiCoO_2$ suspensions. Fig 7a shows that, 50.0 mg/L freshly suspended (1-hr) $LiCoO_2$ NPs induced significantly longer DNA tails in comparison to those resulted from their dissolved Co^{2+} counterpart of 112 µg/L ($P < 0.05$, non-parametric ANOVA test with Dunn's multiple comparison test). Yet, no significant difference was observed in DNA tail length between $LiCoO_2$ NPs and their corresponding amount of dissolved Co^{2+} when the suspension is 48-hr old (Fig 7b). Together with solution H_2O_2 production in the 1-hr old $LiCoO_2$ NP suspensions that decayed over time (Fig 2a), we hypothesize that the increase in DNA tail length induced by fresh $LiCoO_2$ suspension may have resulted from the extracellular H_2O_2 generated in the fresh $LiCoO_2$ suspensions, which led to additional DNA damage that cannot be accounted for by the presence of Co^{2+} alone. H_2O_2, an uncharged species that can penetrate membranes[47] and enter bacterial cells, has been known to induce cellular stress whenever it is present in their extracellular habitat. With as little as 1 µM of intracellular H_2O_2, crippling levels of DNA damage has been reported in *E. coli*.[48]

In addition to examine the resulting DNA damage in bacterial cells, gene expression changes related to bacterial oxidative stress, metal regulation and DNA repair mechanisms were also evaluated to help understand the biological response to both $LiCoO_2$ NP suspensions and their corresponding amount of Co^{2+} released. The specific functions of each gene examined are included in Table S1 in the ESI. *B. subtilis* was exposed to fresh (1 hr) and aged (48 hr) suspensions of $LiCoO_2$ NPs and Co^{2+} at 5 and 50 mg/L concentration levels to complement the DNA damage analysis. The heat map in Table 2 shows that, among the three categories of genes examined, the ones related to oxidative stress pathways are most severely altered. None of the genes related to metal regulation or DNA repair is significantly changed compared to control.

In a previous global analysis of oxidative stress genes[57], it has been demonstrated that protection against H_2O_2 in *B. subtilis* was largely mediated by the induction of proteins controlled by the PerR regulon, representing the primary stress response. Among members of the PerR regulon, only *katA, mrgA,* and *zosA* can be strongly induced by the H_2O_2 treatment.[58,59] Remarkably, *katA* and *mrgA*, encoding the vegetative catalase, KatA, and the metalloregulation DNA-binding stress protein, MrgA, respectively, are the most significantly altered genes in all testing conditions in our study. A previous study examining changes in the CAT gene in a benthic-dwelling organism, *C. riparius*, upon exposure up to 100 mg/L $LiCoO_2$ has also reported significant down regulation of the CAT genes.[26] In addition, *tpx,* another gene that is significantly changed in Fig 8a and 8b, encodes proteins that has been suggested to be a thiol peroxidase, has been linked to peroxide detoxification.[57]

Fig 8 shows key comparisons of genes that were significantly changed upon exposure to $LiCoO_2$ and/or corresponding amount of Co^{2+} (see Fig S8 for plots including all genes). Interestingly, Fig 8a shows that 1-hr old $LiCoO_2$ NPs induced different levels of changes in the expressions of the *katA*, *mrgA* and *tpx* genes compared to Co^{2+} alone. Yet 48-hr aged $LiCoO_2$ NPs do not induce differences in gene expression levels when compared to Co^{2+} (Fig 8b). Cobalt exposure has been linked to negative impact on catalase expression in several multicellular organisms.[26,60]. Among bacterial species, Co-induced stress has been attributed to the disruption of heme synthesis and the ligand coordination in Fe-S protein clusters.[52,61–64] More specifically, a study of Co-induced stress in *E. coli* has demonstrated that OxyR (a homologue to PerR in *B. subtilis*)-mediated responses were observed as a consequence of Fe-S homeostasis imbalance upon Co^{2+} exposure.[65] Therefore, the changes in gene expression levels upon Co^{2+} exposure in Fig 8 are expected in *B. subtilis*. However, the additional impact from freshly-suspended $LiCoO_2$ NP in Fig 8a suggest the presence of additional factors. We attribute that the observed differences are likely the results of H_2O_2 generated in fresh (1-hr) $LiCoO_2$ NP suspensions, which decreases over 48 hours. On the other hand, a greater concentration of Co^{2+} is released in the aged $LiCoO_2$ suspension, which may have contributed to the greater

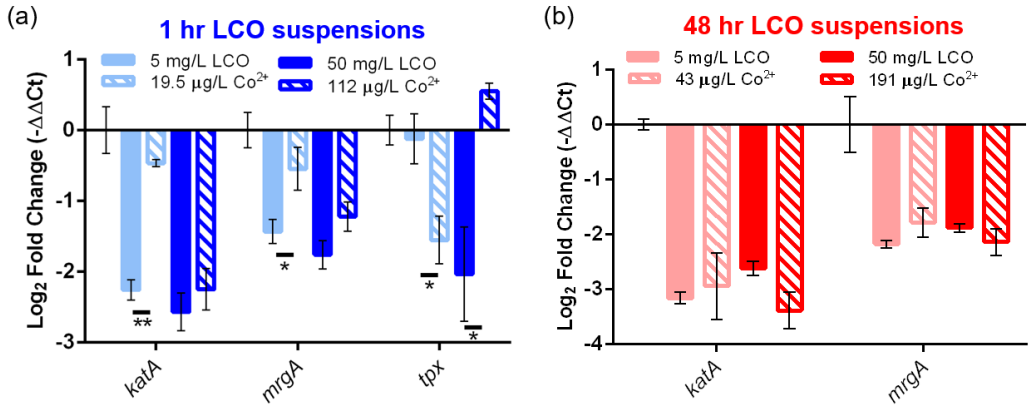

Figure 8. Comparisons of significantly changed genes in *B. subtilis* upon $LiCoO_2$ or Co^{2+} exposure. Solid bars refer to the response to $LiCoO_2$ NPs and stripped bars represent the corresponding amount of Co ions. Error bars represent standard error of means (n = 4, ** for $P < 0.01$, and * for $P < 0.05$ according to one-way ANOVA with Tukey's multiple comparisons test).

impacts in these oxidative stress genes in the 48-hr old $LiCoO_2$ suspensions (Fig 8b). We also note that, interestingly, although we have observed an increase in intracellular O_2^- signals using a fluorescence probe (Fig 6a), no significant fold changes in the oxidative stress gene *sodA*, related to the superoxide anion, was observed. This difference could be due to the dynamic conversions of ROS in the intracellular environment. We note that the formation of intracellular superoxide from molecular oxygen could be catalyzed by Co^{2+},[56] and unlike H_2O_2, superoxide anion is not membrane permeant. The gene expression profile especially highlights the differences in cellular response to the stimulus of H_2O_2 (*katA, mrgA* and *tpx*), likely in response to the abiotic generation of H_2O_2 in the growth medium.

Oxidative stress in bacteria has been a well-reviewed area.[32,45,48,66] It was recently proposed that induction of the OxyR regulon (PerR for *B. subtilis*) is one of the most reliable markers for oxidative stress in bacteria, as it is the bacterial detection system for intracellular H_2O_2.[66] We note that the connection between the generation of abiotic ROS in growth media and the intracellular ROS detected in model organism needs to be carefully established. Previous study has demonstrated that even when NPs do not generate abiotic ROS spontaneously, they may still induce intracellular ROS in mammalian cells and induce mitochondrial apoptosis.[1] Here, we demonstrate that the abiotic ROS (H_2O_2 in this case) generated in the process of NP transformation in solution can also trigger intracellular ROS and lead to additional oxidative stress responses in cells. Since both the abiotic ROS generation and intracellular ROS responses are dynamic, their correlation and interdependence can only be probed properly when both processes are monitored over time.

Conclusion

Altogether, our detailed analysis reveals that $LiCoO_2$ NPs in aqueous growth medium can spontaneously release cobalt ions and generate H_2O_2 when freshly suspended in solution. An initial burst of H_2O_2 in solution is followed by a subsequent decrease over time, while cobalt ion concentration increases over the time period monitored. Solution ROS generation from nanomaterials has previously been demonstrated largely in semiconductors and photosensitive materials.[1,3,19] $LiCoO_2$, as a model complex metal oxide, has not been previously identified as an ROS generator. The half reaction of $LiCoO_2$ reduction to generate Co^{2+} in water has a standard reduction potential of $E^0 = +2.14$ V vs. SHE, which is likely to drive the oxidation half reaction of H_2O to form H_2O_2 ($E^0 = -1.76$ V vs. SHE) thermodynamically. Therefore, it is critical to identify and quantify abiotic ROS formation, as well as to develop principles to predict biological impact upon NP exposure. We note that the fate of solution ROS, depending on its identity, can also be further influenced by media constituents, for instance pyruvate has been shown to sequester H_2O_2 to remediate cytotoxicity in mammalian cells,[67] and radical scavenger, Trolox, or serum proteins can mitigate lipid peroxidation by ROS generated from TiO_2 nanoparticles.[68]

Overall, our study has revealed the intriguing dynamic oxidative stress responses in *B. subtilis* in response to the aqueous transformation of $LiCoO_2$. Although NP toxicity through dissolution and associated release of toxic ions into solution has been a well-established mechanism to organisms,[18,69,70] the spontaneous formation of ROS in aqueous media by NPs coupled to ion release has been less investigated,[1,3] especially in the absence of light or other energy sources. By using a bacterial model, and allowing the NP suspensions to transform independently from biological exposure, we successfully demonstrate the biological impacts of both ion release and the spontaneous formation of abiotic ROS by $LiCoO_2$. By acknowledging the dynamic nature of nanomaterial transformation which may trigger different subtle oxidative stress responses in organisms, we have designed the experiments that allow us to evaluate these variables independently. Although our attempt at tackling the dynamic process of nanomaterial transformation is coarse in this work (two time points), the information revealed provides us with insights into the subtle molecular-level responses in model organisms that have previously been obscured. Our approach is a crucial step towards a new way to evaluate nanotoxicity of complex metal oxides that will allow us to predict the environmental and biological impacts of these nanomaterials more accurately.

Materials and Methods

Nanoparticle synthesis and transformation in bacterial growth medium

Synthesis of lithium cobalt oxide nanomaterials. We synthesized sheet-like nanoparticles of Li_xCoO_2 as described in detail in previous publications.[29,30] Only a brief description is provided here. First $Co(OH)_2$ nanoparticles were prepared through a precipitation between lithium hydroxide, LiOH, and cobalt nitrate hexahydrate, $Co(NO_3)_2{\cdot}6H_2O$. The $Co(OH)_2$ precursor nanoparticles were then transformed into lithium cobalt oxide, Li_xCoO_2 by addition to a molten salt flux of $LiNO_3$:LiOH. The reaction in the molten salt flux was allowed to continue for 30 minutes, then quenched with water. The isolated precipitate was dried at 30 °C in a vacuum oven overnight, and stored in a glovebox under argon atmosphere when not in use.

Characterization of as-synthesized lithium cobalt oxide nanoparticles. Scanning electron micrographs of the pristine particles were taken using a Leo Supra55 VP scanning electron microscope, 3 kV electron energy, using a secondary electron detector. Nanoparticle surface area was analyzed by nitrogen physisorption Brunauer–Emmett–Teller (BET) analysis using a Micromeritics Gemini VII 2390 Surface Area Analyzer. Powder X-Ray Diffraction patterns were obtained using a Bruker D8 ADVANCE powder diffractometer with a Cu Kα source and a Lynxeye detector. Dynamic light scattering (DLS) and zeta potential (ZP) measurements were taken using a Malvern Zetasizer Nano ZS. Transmission electron micrographs of fresh $LiCoO_2$ nanomaterial were obtained by dispersing 10 µL of a 1000x diluted stock $LiCoO_2$ suspension in Nanopure water on a Ted Pella copper grid with carbon type-B 300 mesh. The sample was then characterized on a JEOL 2100 Cryo TEM with LaB_6 emitter operated at 200 keV.

Lithium cobalt oxide nanoparticle transformation in growth medium. A minimal bacterial growth medium (11.6 mM NaCl, 4.0 mM KCl, 1.4 mM $MgCl_2$, 2.8 mM Na_2SO_4, 2.8 mM NH_4Cl, 88.1 µM Na_2HPO_4, 50.5 µM $CaCl_2$, 10 mM HEPES, and 10 mM dextrose) was used to represent a typical low nutrient natural environment and to reduce nanoparticle aggregation induced by proteins and amino acids. All experiments were conducted in this medium unless otherwise noted. Stock suspensions of $LiCoO_2$ in the growth medium for chemical transformation analysis were prepared at concentrations of 1000 mg/L by adding 2 mg of $LiCoO_2$ to 2 mL of medium. The suspensions were sonicated in a bath sonicator for 15 min and then incubated on a rotating plate at room temperature for either one hour (for "1-hr" $LiCoO_2$ samples) or 48 hours (for "48-hr" $LiCoO_2$ samples). After the incubation period, samples were diluted in the minimal medium to desirable concentrations for further analysis or bacterial exposure.

To quantify the cobalt ions released from the $LiCoO_2$ after aging, 5 and 50 mg/L diluted $LiCoO_2$ solutions prepared from the 1000 mg/L stock were centrifuged at 4000 ×*g* for 10 min. A fraction of the supernatant was removed and ultra-centrifuged at 200,000 ×*g* for 30 min. The supernatant was then removed to measure for cobalt ion content using the Inductively Coupled Plasma-Mass Spectrometry (ICP-MS), as done previously.[39]

Abiotic ROS generation from lithium cobalt oxide nanoparticles

Solution hydrogen peroxide detection. To detect the formation of hydrogen peroxide, Amplex Red® reagent (Thermo Fisher) was used according to the manufactural procedure. Amplex Red reagent and 0.2 U/mL Horseradish Peroxidase (HRP) were mixed with either standard hydrogen peroxide solutions, or $LiCoO_2$ suspensions at various concentrations to incubate in the dark at room temperature for 30 minutes.[71] Fluorescence intensity was measured (535 nm / 590 nm) from a series of hydrogen peroxide standards to construct a calibration curve for the quantification of solution hydrogen peroxide generated in $LiCoO_2$ suspensions.

Solution singlet oxygen formation. The singlet oxygen sensor green (SOSG) (Thermo Fisher) can be used to detect the presence of singlet oxygen in solution by reacting specifically to singlet oxygen.[19] $LiCoO_2$ suspension were mixed with the SOSG stock solution in a 0.1M HEPES buffer (pH 7.2). The generation of singlet oxygen was evaluated by measuring fluorescence at λ_{ex} = 480 nm and λ_{em} = 528 nm on a 96-well fluorescence plate reader. Fluorescence intensity was background corrected and normalized to those from control wells.

Solution superoxide detection. The formation of superoxide in $LiCoO_2$ suspension can be monitored by measuring the reduction of nitro blue tetrazolium (NBT).[34,35] An NBT stock solution was mixed with $LiCoO_2$ suspensions and incubated at room temperature in the dark for 1 hour. The supernatant of the mixture was obtained through centrifugation (12,000 ×*g,* 5 min), and analyzed on a spectrophotometer at 259 nm. The formation of superoxide in solution is often indicated by the reduction in the peak intensity at 259 nm, resulted from the depletion of NBT upon reacting with superoxide.

Bacterial culture and lithium cobalt oxide nanoparticle exposure

Bacillus subtilis SB491 was purchased from the Bacillus Genetic Stock Center (Columbus, OH). Bacterial colonies were grown in solid lysogeny broth (LB) agar plates, and inoculated in LB growth medium overnight at 37 °C.

Lithium cobalt oxide nanoparticle toxicity to *B. subtilis*. Growth-based viability (GBV) was performed to assess the bacterial viability in the presence of aged $LiCoO_2$.[40] *B. subtilis* was inoculated and grew in liquid LB at 37 °C overnight and harvested at mid-log phase. The cell pellets were then washed with Dulbecco phosphate-buffered saline (D-PBS) and resuspended in minimal medium with dextrose. The bacterial culture was then diluted to an $OD_{600\ nm}$ of 0.05 with minimal medium. Bacterial culture at OD 0.05 was exposed to desired $LiCoO_2$ suspension conditions for 30 minutes while agitated, and reinoculated in fresh LB media for 16 hours. The growth curves were compared and analyzed to assess the impact of $LiCoO_2$ or Co^{2+} to bacterial viability.

Intracellular fluorescence assays

General intracellular ROS formation. To detect the formation of intracellular reactive oxygen species in general, the non-specific ROS fluorescence probe, 2',7'-dichlorodihydrofluorescein diacetate,

$DCFH_2$-DA, was used according to manufactural procedure. Bacterial cells were harvested at mid-log phase and adjusted to OD_{600} of 0.2. $DCFH_2$-DA stock solution was added to the cell culture to a final dye concentration of 20 µM, followed by an incubation at 37 °C for 1 hour in the dark. After incubation, cells pellets were resuspended in fresh minimal medium to eliminate the unreacted dye. $LiCoO_2$ suspensions were added to the dye-loaded cells and incubated with cells for 30 minutes. Lastly, the $LiCoO_2$-treated bacterial culture were washed and resuspended in fresh minimal medium for OD_{600} and fluorescence measurements (485 nm / 525 nm).

Dihydroethidium assay for intracellular superoxide. To detect the formation of intracellular superoxide formation, Dihydroethidium (DHE) (Sigma Aldrich) was used.[3,44] Bacterial cell cultures suspended in minimal medium with dextrose at OD_{600} 0.6 were incubated with 5 µM DHE solution in the dark at 37 °C for 30 minutes. $LiCoO_2$ suspensions at various concentrations were added to the dye-loaded cell cultures and incubated with cells for 30 minutes. Bacterial cell pellets were then centrifuged and resuspended in fresh minimal medium for OD_{600} and fluorescence measurements (500 nm / 580 nm).

Co^{2+} internalization in bacterial cells. To monitor the internalization of Co^{2+}, a $DCFH_2$-DA derivative dye, Newport Green™ (Thermo Fisher) was used.[39] Bacterial culture were adjusted to OD_{600} 0.2 in minimal medium with dextrose, and incubated at 37 °C for 1 hour in the dark. After washing off the excessive dye and resuspending in fresh medium, the cells were exposed to $LiCoO_2$ suspension for 30 minutes. After washing and resuspending in fresh medium, OD_{600} and fluorescence intensity was recorded (505 nm / 535 nm).

All intracellular fluorescence assays were first normalized over cell density (F/OD_{600}) to correct for any discrepancies in the number of bacterial cells. The corrected fluorescence intensities were then normalized over control to yield a "fold change".

Bacterial DNA damage

Bacterial double-strand DNA breakage upon $LiCoO_2$ exposure as an indication for DNA damage has been studied using the single-cell gel electrophoresis method, as previously described.[11,42] Briefly, 10 µL of diluted $LiCoO_2$ exposed cells at OD_{600} 0.05 were mixed in 100 µL Low Melting Agar, and placed on a FLARE™ Slide (Trevigen, MD). Slides were incubated at 4 °C for 10 minutes to solidify, followed by the addition of a second LMA gel layer containing a 0.5 % lysozyme solution. Once the second layer is solidified, the slide was incubated at 37 °C for 30 minutes in the dark, followed by overnight immersion in a lysing solution (2.5 M NaCl, 100.0 mM EDTA, 10.0 mM Tris -HCl, 1% sodium N-lauryl sarcosine, 0.6% Triton® X-100, pH 10.0), and an enzyme digestion solution (2.5 M NaCl, 10.0 mM EDTA, 10.0 mM Tris-HCl, and 0.5 mg/mL proteinase K, pH 7.4) at 37 °C for 2 hours. Slide then underwent electrophoresis in a chilled opaque electrophoresis tank with sodium acetate – Tris electrophoretic buffer at pH 9.0 at 12 V for 30 minutes in the dark. The slide was then dehydrated in a sequence of solutions of 1 M ammonium acetate in ethanol (20 minutes), absolute ethanol (30 minutes), and 70% ethanol (10 minutes), and dried in ambient air for 5 minutes. Lastly, the slides were rehydrated in 20 µL of DMSO solutions (5% DMSO, 10 mM $Na_2H_2PO_4$) and stained with 20 µL of 1 µM YOYO-1 dye in 5% DMSO and imaged with a fluorescence microscope (λ_{ex} = 491 nm, λ_{em} = 509 nm). Positive controls have been previously conducted using kanamycin and a cationic polymer, poly(allylamine hydrochloride).

Changes in bacterial gene expression

To study the changes in gene expression levels in *B. subtilis* upon exposure to different age and concentrations of $LiCoO_2$ suspensions or to corresponding amount of Co^{2+} released, bacterial cultures were harvested at mid-log phase and adjusted to OD_{600} of 0.2 in the minimal growth medium, and incubated with various nanoparticle or ion treatments at 37 °C for 30 minutes. After incubation, the exposed bacterial cells were harvested by spinning and flash-freezing, and stored in -80 °C until RNA extraction. Four biological replicates were collected for the controls and each treatment groups.

A detailed description for RNA extraction is provided in the ESI. The same qPCR procedure has also been previously reported.[42] Briefly, to synthesize complementary deoxyribonucleic acid (cDNA) following Invitrogen's protocols and the iCycler base module of an iQ5 Multicolor Real-Time, extracted RNA was mixed with Master Mix 1 (random primers (Invitrogen, 48190-011) and dNTP (Invitrogen, 18427013)) for 5 minutes at 65 °C, then chilled on ice for 1 minute. Then Master mix 2 (5x- First Strand Buffer, Dithiothreitol, RNaseOUT™ recombinant ribonuclease inhibitors (Invitrogen, 10777019), and Superscript RT III reverse transcriptase (Invitrogen, 18080-044)) was added to the reaction in an iQ5 Multicolor Real-Time PCR Detection System at 25 °C for 5 minutes, 50 °C for 60 minutes, 70 °C for 15 minutes for random primer extension. The resulting cDNA samples were characterized on a NanoDrop UV-vis spectrometer and stored at -20 °C until qPCR analysis.

Target genes relevant to oxidative stress, metal homeostasis and DNA repair have been selected for *B. subtilis*. Table S1 in ESI provides detailed information regarding the functions of the genes and the sequences of the primers. For qPCR using an iQ5 real-time PCR detection system (Bio-Rad Laboratories) with SYBR Green for the fluorescent intercalating dye (iTaq™ Universal SYBR® Green Supermix, Bio-Rad), manufactural protocol was followed. cDNA, primers and SYBR® Green Supermix (Bio-Rad) were combined to react in a qPCR 96-well plate. The reaction started at 95 ˚C for 10 minutes to denature the DNA, followed by 40-times temperature cycles of amplification of 15 s at 95 ˚C and 30 s at 60 ˚C. The gene expression data was processed by normalizing the raw threshold cycle (C_t) numbers against the output of a housekeeping gene, *arsR*. Each qPCR reaction was duplicated, and each gene analysis included four biological replicates.

Statistical analysis

Nanomaterial characterizations and quantitative analysis (e.g. ICP-MS) were carried out with three technical replicates and three analytical replicates. Biological exposure, intracellular ROS, viability, and gene expression experiments throughout the study were carried out at least in triplicates ($n \geq 3$). Depending on the parameters

compared in each analysis, different statistical tests were used. Details of the analysis are provided in each figure caption.

Bacterial cells used for single cell gel-electrophoresis analysis were from 4 biological replicates of nanoparticle or ion exposure. DNA tail length data from different replicates were deemed identical to be combined only when the tail lengths analysis from the control groups were not tested to be statistically different ($p > 0.05$). Merged DNA tail length data was tested for normality using the D'Agostino & Pearson normality test first, followed by non-parametric Kruskal-Wallis tests with Dunn's multiple comparisons test.

Conflicts of interest

There are no conflicts to declare.

Acknowledgements

This material is based upon work supported by the National Science Foundation under Grant No. CHE-2001611, the NSF Center for Sustainable Nanotechnology (CSN). The CSN is part of the Centers for Chemical Innovation Program. M.G. and P.L. acknowledge the generosity of Terry Lindstrom for The Lindstrom Family Research Fund through Augsburg University. E.D.L. is supported by the National Science Foundation Graduate Research Fellowship Program under grant no. DGE-1747503. Additional support to E.D.L. was also provided by the Graduate School and the Office of the Vice Chancellor for Research and Graduate Education at the University of Wisconsin−Madison with funding from the Wisconsin Alumni Research Foundation. The authors thank Michael P. Schwartz for helpful discussions. The authors gratefully acknowledge use of facilities and instrumentation supported by NSF through the University of Wisconsin Materials Research Science and Engineering Center (DMR-1720415).

Notes and references

(1) Xia, T.; Kovochich, M.; Brant, J.; Hotze, M.; Sempf, J.; Oberley, T.; Sioutas, C.; Yeh, J. I.; Wiesner, M. R.; Nel, A. E. Comparison of the Abilities of Ambient and Manufactured Nanoparticles to Induce Cellular Toxicity According to an Oxidative Stress Paradigm. *Nano Lett.* **2006**, 6, 1794–1807.

(2) Serpone, N.; Emeline, A. V. Semiconductor Photocatalysis - Past, Present, and Future Outlook. *J. Phys. Chem. Lett*. **2012**, 3, 673–677.

(3) Jayaram, D. T.; Kumar, A.; Kippner, L. E.; Ho, P.-Y.; Kemp, M. L.; Fan, Y.; Payne, C. K. TiO2 Nanoparticles Generate Superoxide and Alter Gene Expression in Human Lung Cells . *RSC Adv.* **2019**, *9*, 25039–25047.

(4) Nel, A.; Xia, T.; Mädler, L.; Li, N. Toxic Potential of Materials at the Nanolevel. *Science*. **2006**, 311, 622–627.

(5) Nitta, N.; Wu, F.; Lee, J. T.; Yushin, G. Li-Ion Battery Materials: Present and Future. *Materials Today*. **2015**, 18, 252–264.

(6) Goodenough, J. B.; Park, K. S. The Li-Ion Rechargeable Battery: A Perspective. *J. Am. Chem. Soc.* **2013**, 135, 1167–1176.

(7) Wang, Y.; Liu, B.; Li, Q.; Cartmell, S.; Ferrara, S.; Deng, Z. D.; Xiao, J. Lithium and Lithium Ion Batteries for Applications in Microelectronic Devices: A Review. *J. Power Sources*. **2015**, 286, 330–345.

(8) Notter, D. A.; Gauch, M.; Widmer, R.; Wäger, P.; Stamp, A.; Zah, R.; Althaus, H.-J. Contribution of Li-Ion Batteries to the Environmental Impact of Electric Vehicles. *Environ. Sci. Technol.* **2010**, *44*, 6550–6556.

(9) Larcher, D.; Tarascon, J.-M. Towards Greener and More Sustainable Batteries for Electrical Energy Storage. *Nat. Chem.* **2014**, *7*, 19–29.

(10) Hang, M. N.; Gunsolus, I. L.; Wayland, H.; Melby, E. S.; Mensch, A. C.; Hurley, K. R.; Pedersen, J. A.; Haynes, C. L.; Hamers, R. J. Impact of Nanoscale Lithium Nickel Manganese Cobalt Oxide (NMC) on the Bacterium Shewanella Oneidensis MR-1. *Chem. Mater.* **2016**, *28*, 1092–1100.

(11) Feng, Z. V.; Miller, B. R.; Linn, T. G.; Pho, T.; Hoang, K. N. L.; Hang, M. N.; Mitchell, S. L.; Hernandez, R. T.; Carlson, E. E.; Hamers, R. J. Biological Impact of Nanoscale Lithium Intercalating Complex Metal Oxides to Model Bacterium B. Subtilis. *Environ. Sci. Nano* **2019**, *6*, 305–314.

(12) Bozich, J.; Hang, M.; Hamers, R.; Klaper, R. Core Chemistry Influences the Toxicity of Multicomponent Metal Oxide Nanomaterials, Lithium Nickel Manganese Cobalt Oxide, and Lithium Cobalt Oxide to Daphnia Magna. *Environ. Toxicol. Chem.* **2017**, *36*, 9.

(13) Yu, Z.; Li, Q.; Wang, J.; Yu, Y.; Wang, Y.; Zhou, Q.; Li, P. Reactive Oxygen Species-Related Nanoparticle Toxicity in the Biomedical Field. *Nanoscale Res. Lett.* **2020**, *15*, 115.

(14) Dayem, A. A.; Hossain, M. K.; Lee, S. Bin; Kim, K.; Saha, S. K.; Yang, G. M.; Choi, H. Y.; Cho, S. G. The Role of Reactive Oxygen Species (ROS) in the Biological Activities of Metallic Nanoparticles. *Int. J. Mol. Sci.* **2017**, *18*, 1–21.

(15) Qiu, T. A.; Gallagher, M. J.; Hudson-Smith, N. V.; Wu, J.; Krause, M. O. P.; Fortner, J. D.; Haynes, C. L. Research Highlights: Unveiling the Mechanisms Underlying Nanoparticle-Induced ROS Generation and Oxidative Stress. *Environ. Sci. Nano* **2016**, *3*, 940–945.

(16) Qiu, T. A.; Clement, P. L.; Haynes, C. L. Linking Nanomaterial Properties to Biological Outcomes: Analytical Chemistry Challenges in Nanotoxicology for the next Decade. *Chem. Commun.* **2018**, *54*, 12787–12803.

(17) Nita, M.; Grzybowski, A. The Role of the Reactive Oxygen Species and Oxidative Stress in the Pathomechanism of the Age-Related Ocular Diseases and Other Pathologies of the Anterior and Posterior Eye Segments in Adults. *Oxid. Med. Cell. Longev.* **2016**, 3164734.

(18) Xia, T.; Kovochich, M.; Liong, M.; Mädler, L.; Gilbert, B.; Shi, H.; Yeh, J. I.; Zink, J. I.; Nel, A. E. Comparison of the Mechanism of Toxicity of Zinc Oxide and Cerium Oxide Nanoparticles Based on Dissolution and Oxidative Stress Properties. *ACS Nano* **2008**, *2*, 2121–2134.

(19) Brunet, L.; Lyon, D. Y.; Hotze, E. M.; Alvarez, P. J. J.; Wiesner, M. R. Comparative Photoactivity and Antibacterial Properties of C60 Fullerenes and Titanium Dioxide Nanoparticles. *Environ. Sci. Technol.* **2009**, *43*, 4355–4360.

(20) Limbach, L. K.; Wick, P.; Manser, P.; Grass, R. N.; Bruinink, A.; Stark, W. J. Exposure of Engineered Nanoparticles to Human Lung Epithelial Cells: Influence of Chemical Composition and Catalytic Activity on Oxidative Stress. *Environ. Sci. Technol.* **2007**, *41*, 4158–4163.

(21) Gunsolus, I. L.; Hang, M. N.; Hudson-Smith, N. V; Buchman, J. T.; Bennett, J. W.; Conroy, D.; Mason, S. E.; Hamers, R. J.; Haynes, C. L. Influence of Nickel Manganese Cobalt Oxide Nanoparticle Composition on Toxicity toward Shewanella Oneidensis MR-1: Redesigning for Reduced Biological Impact. *Environ. Sci. Nano* **2017**, *4*, 636–646.

(22) Horst, A. M.; Vukanti, R.; Priester, J. H.; Holden, P. A. An Assessment of Fluorescence- and Absorbance-Based Assays to Study Metal-Oxide Nanoparticle ROS Production and Effects on Bacterial Membranes. *Small* **2013**, *9*, 1753–1764.

(23) Schmidt, J.; Vogelsberger, W. Dissolution Kinetics of Titanium Dioxide Nanoparticles: The Observation of an Unusual Kinetic Size Effect. *J. Phys. Chem. B* **2006**, *110*, 3955–3963.

(24) Cui, Y.; Melby, E. S.; Mensch, A. C.; Laudadio, E. D.; Hang, M. N.; Dohnalkova, A.; Hu, D.; Hamers, R. J.; Orr, G. Quantitative Mapping of Oxidative Stress Response to Lithium Cobalt Oxide Nanoparticles in Single Cells Using Multiplexed in Situ Gene Expression Analysis. *Nano Lett.* **2019**, *19*, 1990–1997.

(25) Melby, E. S.; Cui, Y.; Borgatta, J.; Mensch, A. C.; Hang, M. N.; Chrisler, W. B.; Dohnalkova, A.; Van Gilder, J. M.; Alvarez, C. M.; Smith, J. N.; Hamers, R. J.; Orr, G. Impact of Lithiated Cobalt Oxide and Phosphate Nanoparticles on Rainbow Trout Gill Epithelial Cells. *Nanotoxicology* **2018**, *12*, 1166–1181.

(26) Niemuth, N. J.; Curtis, B. J.; Hang, M. N.; Gallagher, M. J.; Fairbrother, D. H.; Hamers, R. J.; Klaper, R. D. Next-Generation Complex Metal Oxide Nanomaterials Negatively Impact Growth and Development in the Benthic Invertebrate Chironomus Riparius upon Settling. *Environ. Sci. Technol.* **2019**, *53*, 3860–3870.

(27) Feng, Z. V.; Gunsolus, I. L.; Qiu, T. A.; Hurley, K. R.; Nyberg, L. H.; Frew, H.; Johnson, K. P.; Vartanian, A. M.; Jacob, L. M.; Lohse, S. E.; Torelli, M. D.; Hamers, R. J.; Murphy, C. J.; Haynes, C. L. Impacts of Gold Nanoparticle Charge and Ligand Type on Surface Binding and Toxicity to Gram-Negative and Gram-Positive Bacteria. *Chem. Sci.* **2015**, *6*, 5186–5196.

(28) Hang, M. N.; Hudson-Smith, N. V; Clement, P. L.; Zhang, Y.; Wang, C.; Haynes, C. L.; Hamers, R. J. Influence of Nanoparticle Morphology on Ion Release and Biological Impact of Nickel Manganese Cobalt Oxide (NMC) Complex Oxide Nanomaterials. *ACS Appl. Nano Mater.* **2018**, *1*, 1721–1730.

(29) Laudadio, E. D.; Ilani-Kashkouli, P.; Green, C. M.; Kabengi, N. J.; Hamers, R. J. Interaction of Phosphate with Lithium Cobalt Oxide Nanoparticles: A Combined Spectroscopic and Calorimetric Study. *Langmuir* **2019**, *35*, 16640–16649.

(30) Laudadio, E. D.; Bennett, J. W.; Green, C. M.; Mason, S. E.; Hamers, R. J. Impact of Phosphate Adsorption on Complex Cobalt Oxide Nanoparticle Dispersibility in Aqueous Media. *Environ. Sci. Technol.* **2018**, *52*, 10186–10195.

(31) Abbaspour-Tamijani, A.; Bennett, J. W.; Jones, D. T.; Cartagena-Gonzalez, N.; Jones, Z. R.; Laudadio, E. D.; Hamers, R. J.; Santana, J. A.; Mason, S. E. DFT and Thermodynamics Calculations of Surface Cation Release in LiCoO2. *Appl. Surf. Sci.* **2020**, *515*, 145865.

(32) Imlay, J. Diagnosing Oxidative Stress in Bacteria: Not as Easy as You Might Think. *Curr. Opin. Microbiol.* **2015**, *24*, 124–131.

(33) Grisham, M. B. Methods to Detect Hydrogen Peroxide in Living Cells: Possibilities and Pitfalls. *Comp. Biochem. Physiol. - A Mol. Integr. Physiol.* **2013**, *165*, 429–438.

(34) Angelé-Martínez, C.; Goodman, C.; Brumaghim, J. Metal-Mediated DNA Damage and Cell Death: Mechanisms, Detection Methods, and Cellular Consequences. *Metallomics* **2014**, *6*, 1358–1381.

(35) Jayaram, D. T.; Runa, S.; Kemp, M. L.; Payne, C. K. Nanoparticle-Induced Oxidation of Corona Proteins Initiates an Oxidative Stress Response in Cells. *Nanoscale* **2017**, *9*, 7595–7601.

(36) Fernández-Castro, P.; Vallejo, M.; San Román, M. F.; Ortiz, I. Insight on the Fundamentals of Advanced Oxidation Processes: Role and Review of the Determination Methods of Reactive Oxygen Species. *J. Chem. Technol. Biotechnol*. **2015**, *90*, 796–820.

(37) Bartosz, G. Use of Spectroscopic Probes for Detection of Reactive Oxygen Species. *Clinica Chimica Acta*. **2006**, *368*, 53–76.

(38) Gunsolus, I. L.; Hang, M. N.; Hudson-Smith, N. V.; Buchman, J. T.; Bennett, J. W.; Conroy, D.; Mason, S. E.; Hamers, R. J.; Haynes, C. L. Influence of Nickel Manganese Cobalt Oxide Nanoparticle Composition on Toxicity toward Shewanella Oneidensis MR-1: Redesigning for Reduced Biological Impact. *Environ. Sci. Nano* **2017**, *4*, 636–646.

(39) Clement, P. L.; Kuether, J. E.; Borgatta, J. R.; Buchman, J. T.; Cahill, M. S.; Qiu, T. A.; Hamers, R. J.; Feng, Z. V.; Haynes, C. L. Cobalt Release from a Nanoscale Multiphase Lithiated

Cobalt Phosphate Dominates Interaction with Shewanella Oneidensis MR-1 and Bacillus Subtilis SB491. *Chem. Res. Toxicol.* **2020**, *33*, 806–816.

(40) Qiu, T. A.; Nguyen, T. H. T.; Hudson-Smith, N. V.; Clement, P. L.; Forester, D.-C.; Frew, H.; Hang, M. N.; Murphy, C. J.; Hamers, R. J.; Feng, Z. V.; Haynes, C. L. Growth-Based Bacterial Viability Assay for Interference-Free and High-Throughput Toxicity Screening of Nanomaterials. *Anal. Chem.* **2017**, *89*, 2057–2064.

(41) Zhao, J.; Bertoglio, B. A.; Devinney, M. J.; Dineley, K. E.; Kay, A. R. The Interaction of Biological and Noxious Transition Metals with the Zinc Probes FluoZin-3 and Newport Green. *Anal. Biochem.* **2009**, *384*, 34–41.

(42) Qiu, T. A.; Guidolin, V.; Hoang, K. N. L.; Pho, T.; Carra', A.; Villalta, P. W.; He, J.; Yao, X.; Hamers, R. J.; Balbo, S.; Feng, Z. V.; Haynes, C. L. Nanoscale Battery Cathode Materials Induce DNA Damage in Bacteria. *Chem. Sci.* **2020**, 11 (41), 11244–11258.

(43) F.; Stanicka, J.; Cotter, T. G. Recent Advances in Reactive Oxygen Species Measurement in Biological Systems. *Trends Biochem. Sci.* **2013**, *38*, 556–565.

(44) Dikalov, S. I.; Harrison, D. G. Methods for Detection of Mitochondrial and Cellular Reactive Oxygen Species. *Antioxidants and Redox Signaling*. **2014**, *20,* 372–382.

(45) Imlay, J. A. Pathways of Oxidative Damage. *Annu. Rev. Microbiol.* **2003**, *57*, 395–418.

(46) Nogueira, V.; Hay, N. Molecular Pathways: Reactive Oxygen Species Homeostasis in Cancer Cells and Implications for Cancer Therapy. *Clin. Cancer Res.* **2013**, *19*, 4309–4314.

(47) Bienert, G. P.; Schjoerring, J. K.; Jahn, T. P. Membrane Transport of Hydrogen Peroxide. *Biochim. Biophys. Acta - Biomembr.* **2006**, *1758*, 994–1003.

(48) Imlay, J. A. Cellular Defenses against Superoxide and Hydrogen Peroxide. *Annu. Rev. Biochem.* **2008**, *77*, 755–776.

(49) Lloyd, D. R.; Carmichael, P. L.; Phillips, D. H. Comparison of the Formation of 8-Hydroxy-2'-Deoxyguanosine and Single- and Double-Strand Breaks in DNA Mediated by Fenton Reactions. *Chem. Res. Toxicol.* **1998**, *11*, 420–427.

(50) Solanky, D.; Haydel, S. E. Adaptation of the Neutral Bacterial Comet Assay to Assess Antimicrobial-Mediated DNA Double-Strand Breaks in Escherichia Coli. *J. Microbiol. Methods* **2012**, *91*, 257–261.

(51) Liao, W.; McNutt, M. A.; Zhu, W.-G. The Comet Assay: A Sensitive Method for Detecting DNA Damage in Individual Cells. *Methods* **2009**, *48*, 46–53.

(52) Lemire, J. A.; Harrison, J. J.; Turner, R. J. Antimicrobial Activity of Metals: Mechanisms, Molecular Targets and Applications. *Nat. Rev. Microbiol.* **2013**, *11*, 371–384.

(53) Giannousi, K.; Lafazanis, K.; Arvanitidis, J.; Pantazaki, A.; Dendrinou-Samara, C. Hydrothermal Synthesis of Copper Based Nanoparticles: Antimicrobial Screening and Interaction with DNA. *J. Inorg. Biochem.* **2014**, *133*, 24–32.

(54) Mitchell, S. L.; Carlson, E. E. Tiny Things with Enormous Impact: Nanotechnology in the Fight Against Infectious Disease. *ACS Infect. Dis.* **2018**, *4*, 1432–1435.

(55) Lloyd, D. R.; Phillips, D. H. Oxidative DNA Damage Mediated by Copper(II), Iron(II) and Nickel(II) Fenton Reactions: Evidence for Site-Specific Mechanisms in the Formation of Double-Strand Breaks, 8-Hydroxydeoxyguanosine and Putative Intrastrand Cross-Links. *Mutat. Res. - Fundam. Mol. Mech. Mutagen.* **1999**, *424*, 23–36.

(56) Leonard, S.; Gannett, P. M.; Rojanasakul, Y.; Schwegler-Berry, D.; Castranova, V.; Vallyathan, V.; Shi, X. Cobalt-Mediated Generation of Reactive Oxygen Species and Its Possible Mechanism. *J. Inorg. Biochem.* **1998**, *70*, 239–244.

(57) Mostertz, J.; Scharf, C.; Hecker, M.; Homuth, G. Transcriptome and Proteome Analysis of Bacillus Subtilis Gene Expression in Response to Superoxide and Peroxide Stress. *Microbiology* **2004**, *150*, 497–512.

(58) Helmann, J. D.; Wu, M. F. W.; Gaballa, A.; Kobel, P. A.; Morshedi, M. M.; Fawcett, P.; Paddon, C. The Global Transcriptional Response of Bacillus Subtilis to Peroxide Stress Is Coordinated by Three Transcription Factors. *J. Bacteriol.* **2003**, *185*, 243–253.

(59) Fuangthong, M.; Herbig, A. F.; Bsat, N.; Helmann, J. D. Regulation of the Bacillus Subtilis Fur and PerR Genes by PerR: Not All Members of the PerR Regulon Are Peroxide Inducible. *J. Bacteriol.* **2002**, *184*, 3276–3286.

(60) Kubrak, O. I.; Husak, V. V.; Rovenko, B. M.; Storey, J. M.; Storey, K. B.; Lushchak, V. I. Cobalt-Induced Oxidative Stress in Brain, Liver and Kidney of Goldfish Carassius Auratus. *Chemosphere* **2011**, *85*, 983–989.

(61) Thorgersen, M. P.; Downs, D. M. Cobalt Targets Multiple Metabolic Processes in Salmonella Enterica. *J. Bacteriol.* **2007**, *189*, 7774–7781.

(62) Fantino, J. R.; Py, B.; Fontecave, M.; Barras, F. A Genetic Analysis of the Response of Escherichia Coli to Cobalt Stress. *Environ. Microbiol.* **2010**, *12*, 2846–2857.

(63) Ranquet, C.; Ollagnier-de-Choudens, S.; Loiseau, L.; Barras, F.; Fontecave, M. Cobalt Stress in Escherichia Coli: The Effect on the Iron-Sulfur Proteins. *J. Biol. Chem.* **2007**, *282*, 30442–30451.

(64) Majtan, T.; Frerman, F. E.; Kraus, J. P. Effect of Cobalt on Escherichia Coli Metabolism and Metalloporphyrin Formation. *BioMetals* **2011**, *24*, 335–347.

(65) Barras, F.; Fontecave, M. Cobalt Stress in Escherichia Coli and Salmonella Enterica: Molecular Bases for Toxicity and Resistance. *Metallomics*. **2011**, *3*, 1130–1134.

(66) Imlay, J. A. Where in the World Do Bacteria Experience Oxidative Stress? *Environ. Microbiol.* **2019**, *21*, 521–530.

(67) Kelts, J. L.; Cali, J. J.; Duellman, S. J.; Shultz, J. Altered Cytotoxicity of ROS-Inducing Compounds by Sodium Pyruvate in Cell Culture Medium Depends on the Location of ROS Generation. *Springerplus* **2015**, *4*, 269.

(68) Runa, S.; Khanal, D.; Kemp, M. L.; Payne, C. K. TiO2 Nanoparticles Alter the Expression of Peroxiredoxin Antioxidant Genes. *J. Phys. Chem. C* **2016**, *120*, 20736–20742.

(69) Dekkers, S.; Williams, T. D.; Zhang, J.; Zhou, J.; Vandebriel, R. J.; De La Fonteyne, L. J. J.; Gremmer, E. R.; He, S.; Guggenheim, E. J.; Lynch, I.; Cassee, F. R.; De Jong, W. H.; Viant, M. R. Multi-Omics Approaches Confirm Metal Ions Mediate the Main Toxicological Pathways of Metal-Bearing Nanoparticles in Lung Epithelial A549 Cells. *Environ. Sci. Nano* **2018**, *5*, 1506–1517.

(70) Schultz, A. G.; Boyle, D.; Chamot, D.; Ong, K. J.; Wilkinson, K. J.; McGeer, J. C.; Sunahara, G.; Goss, G. G. Aquatic Toxicity of Manufactured Nanomaterials: Challenges and Recommendations for Future Toxicity Testing. *Environ. Chem.* **2014**, *11*, 207–226.

(71) Zhao, B, Summers F. A, and Mason, R. P. Photooxidation of Amplex Red to Resorufin: Implications of Exposing the Amplex Red Assay to Light. *Free Radic. Biol. Med.* **2012**, *53*, 1080–1087